sustainability

MDPI

Article

Impact of Deforestation on Land–Atmosphere Coupling Strength and Climate in Southeast Asia

Merja H. Tölle [1,2]

[1] Department of Geography, Justus-Liebig University Giessen, 35390 Giessen, Germany; merja.toelle@geogr.uni-giessen.de

[2] Center of Environmental Systems Research (CESR), University of Kassel, 34117 Kassel, Germany

Received: 3 June 2020; Accepted: 27 July 2020; Published: 30 July 2020

Abstract: Southeast Asia (SEA) is a deforestation hotspot. A thorough understanding of the accompanying biogeophysical consequences is crucial for sustainable future development of the region's ecosystem functions and society. In this study, data from ERA-Interim driven simulations conducted with the state-of-the-art regional climate model COSMO-CLM (CCLM; version 4.8.17) at 14 km horizontal resolution are analyzed over SEA for the period from 1990 to 2004, and during El Niño–Southern Oscillation (ENSO) events for November to March. A simulation with large-scale deforested land cover is compared to a simulation with no land cover change. In order to attribute the differences due to deforestation to feedback mechanisms, the coupling strength concept is applied based on Pearson correlation coefficients. The correlations were calculated based on 10-day means between the latent heat flux and maximum temperature, the latent and sensible heat flux, and the latent heat flux and planetary boundary layer height. The results show that the coupling strength between land and atmosphere increased for all correlations due to deforestation. This implies a strong impact of the land on the atmosphere after deforestation. Differences in environmental conditions due to deforestation are most effective during La Niña years. The strength of La Nina events on the region is reduced as the impact of deforestation on the atmosphere with drier and warmer conditions superimpose this effect. The correlation strength also intensified and shifted towards stronger coupling during El Niño events for both Control and Grass simulations. However, El Niño years have the potential to become even warmer and drier than during usual conditions without deforestation. This could favor an increase in the formation of tropical cyclones. Whether deforestation will lead to a permanent transition to agricultural production increases in this region cannot be concluded. Rather, the impact of deforestation will be an additional threat besides global warming in the next decades due to the increase in the occurrence of multiple extreme events. This may change the type and severity of upcoming impacts and the vulnerability and sustainability of our society.

Keywords: deforestation; agricultural production; oil palm; Southeast Asia; land–atmosphere coupling; ENSO; land use/cover change; Regional Climate Model; sustainability, vulnerability, society; tropical cyclones

1. Introduction

Ongoing climate change is a global problem [1]. Anthropogenic changes in atmospheric gaseous components and land-use changes are the main drivers leading to climate change [2]. Forests play a particular role in land-use changes as they sequester carbon, influence the hydrological and energy cycle, and contribute to floral and faunal diversity. Deforestation occurs all over the world and disturbs the balance. While the forested area has stabilized or is even increasing over Europe and North America [3], deforestation is still ongoing at a fast pace in some areas of South America, Africa, and Southeast Asia [4–7].

Southeast Asia (SEA) is a deforestation hotspot [8], and is currently one of the regions with the highest transformation rate of land surfaces for agricultural use and urban development. Vast areas of cleared land over Indonesia or Malaysia has been transformed into industrial oil palm plantations over the past few decades. For example, about 50% of the deforested land on the Borneo island has been planted with oil palms since 2000 [9]. About 877,000 acres are lost each year. Replanting cleared land by oil palms requires enormous amounts of water [10], which increases the competition for water resources. The impact of this extensive deforestation for agricultural use on SEA's climate is still uncertain. In addition, whether this will lead to a permanent transition to agricultural production, as anticipated in this region, is not clear.

Deforestation modifies the land surface properties, resulting in alterations to surface fluxes such as moisture, heat, and momentum, which directly affect the temperature and ultimately the atmospheric boundary layer [11,12]. These effects are known as biogeophysical impacts acting on local and regional scales. Biogeochemical effects occur via changes in carbon dioxide fluxes, trace gases, and aerosols affecting mainly the global scale. Many studies have shown that these effects interact in a complex way over a range of different temporal and spatial scales, influencing weather and climate [12–19].

The vulnerability of the Southeast Asian region is additionally to extensive deforestation modified by strong climate variability. The South Asian Monsoon and Asian-Australian Monsoon dominate the annual cycle of rainfall, and thereby influence the environmental conditions over large areas of SEA. Monsoon rainfall is important for water supply, agriculture, and natural ecosystems. The South Asian Monsoon and the Asian-Australian Monsoon develop, respectively, during boreal and austral summers through substantial rearrangement of the large-scale atmospheric circulation, which results in a rapid increase in precipitation.

El Niño–Southern Oscillation (ENSO) circulation amplifies the monsoon climate. This can result in drought or flood events [20] depending on the strength of the ENSO phenomenon. However, it is not clear what impact large-scale deforestation may have on ENSO events and if the modified biophysical processes due to ongoing vast deforestation could potentially enhance or dampen the strength of ENSO. The large extent of deforestation in the Southeast Asian region in recent decades, and the projected increase in temperature and drought events in coming decades, increases the importance of quantifying the potential impact of deforestation on local and regional climate also during ENSO events. This importance is highlighted by the fact that ENSO periods influence the annual fluctuations and the intensification rate of tropical cyclones, which are recurring phenomena in the Southeast and East Asian regions [21,22]. El Niños phases are characterized by the formation of stronger and longer lasting typhoons compared to La Niña phases [23]. El Niño events have resulted in an increase in typhoons by more than 40% in previous decades [24]. La Niña events have resulted in a 29% decrease in the number of strong typhoons. Thus, future changes in ENSO as a response to anthropogenic global warming [25] could have significant socioeconomic consequences [26] and unprecedented environmental impacts affecting health, productivity, crop yield, and disease outbreaks for the growing population in the coastal areas of SEA [27].

A regional climate modelling study of large-scale deforestation over SEA in the recent past showed an increase/decrease of temperature/precipitation over the region [28]. It was found that precipitation events have become more intense, and extreme temperatures have become higher after large-scale land clearing. A study based on observational records over the island of Borneo found a strong relationship between forest loss and the increase in temperature and reduction in precipitation [29]. Regional temperature increases differ in magnitude from global warming due to the feedback processes. Changes in regional temperatures on land have been much greater than changes in the global mean temperature [30]. Therefore, quantification of the impact of land cover changes on regional to local climates are relevant for regional land use planning and climate mitigation and adaptation strategies [31]. Thus, changes in feedback processes over land due to forest loss play an essential role, and they depend on the coupling strength between the land and the atmosphere [32]. Hence, the state of the land surface and land–atmosphere feedback could potentially modulate and

amplify extreme climatic events in SEA, and more importantly, during ENSO events. The strength of this coupling might determine the impact the land cover change in the Southeast Asian region.

Earlier studies used land–atmosphere coupling metric for evaluation purposes on air temperature, evapotranspiration flux, and soil moisture [32]. The coincidence metric concentrates on the bivariate dependence structure of two variables, and is insensitive to biases in the means or variances. Here, we use this approach to quantify the change in the land–atmosphere coupling due to deforestation, and during ENSO events. We apply this method to a different set of data alighning with extreme environmental conditions. We consider correlations between maximum air temperatures and latent heat flux, which addresses the soil–moisture–temperature feedback [30], and the feedback into the atmosphere [33]. In the case that the land is covered by vegetation, this metric additionally accounts for the moisture flux capability of the vegetation layer. For example, the water transpiration capability of grass is smaller than that of tropical forest. Correlations are calculated between the sensible and latent heat fluxes as they show the process of the flux partitioning change due to the available energy at the surface. In order to account for the impact of deforestation to the atmospheric boundary layer, we consider the correlations between latent heat flux and height of the planetary boundary layer.

The impact of deforestation on the land–atmosphere coupling strength is studied by analyzing ERA-Interim–driven simulations of the state-of-the-art regional climate model COSMO-CLM during the period from 1990 to 2004 for November to March. Major forest loss occurred in the SEA in this period [34]. Moreover, this study examines the impact of land clearing during ENSO events and provides necessary information for regional land use planning and climate mitigation and adaptation strategies. Section 2 outlines the data and methods used. In Section 3, the results are presented, and Section 4 concludes the study.

2. Data and Methods

2.1. Study Region

The analysis domain in this study was similar to the domain of the Coordinated Regional Downscaling Experiment (CORDEX) of SEA in order to make the present investigation relevant within a wider context. This study domain covered the whole of the maritime continent of SEA, spanning from ~14° S to ~15° N and ~93° E to ~138° E (see Figure 1), with 450 × 240 grid points at a 14 km horizontal resolution. The study area belongs to the maritime equatorial climate region. Seasonal variation in the intertropical convergence zone dominates the regional circulation system characterized by seasonal patterns in precipitation (seasonal monsoon). Further, the region is characterized by variations in the Walker circulation, which occur periodically, potentially resulting in ENSO events. The region is bordered by the Indian Ocean to the west and the Pacific Ocean to the east. The northern part of the study domain belongs to the Indochinese Peninsula, and the south is part of the Northern Territory of Australia. These regions belong to the sub equatorial area with tropical monsoon climate showing a wet and a short dry season.

2.2. Model Data

In order to analyze changes in land–atmosphere coupling due to deforestation and during ENSO phases, data were taken from simulation experiments for SEA with the state-of-the-art regional climate model COSMO-CLM. It is a non-hydrostatic limited-area atmospheric climate model used in its version 4.8.17. The COSMO model [35] was originally developed by the German Weather Service for weather forecast applications and is used in climate mode [36] by the CLM-community. COSMO-CLM was driven by observed climate forcing based on the reanalysis product of ERA-Interim [37] as initial and lateral boundary conditions. The simulations were performed over the period from 1984 to 2004. The first six years of the simulation allows the model to spin-up for balanced soil moisture conditions. Tölle et al. [19] describes the configuration of the model and experiment set-up in detail. Simulation experiments included a control simulation over the SEA domain with current land cover, and a

deforestation simulation, where the forest cover over SEA was replaced by grassland. The control simulation with no land cover change was denoted as Control in this study. The deforestation simulation, named Grass, consisted of grassland and covered the period from 1990 to 2004. The simulation for grassland started from a point at which the climate model was in a dynamic equilibrium. Therefore, it is performed as a restart from the Control simulation in 1990, but with alternative land cover and vegetation parameters accounting for grass. Here, all forest grid cells with plant coverage of more than 80 percent in a grid cell were converted to grassland. Since lateral boundary conditions were not changed, simulated changes could be explained by land cover change.

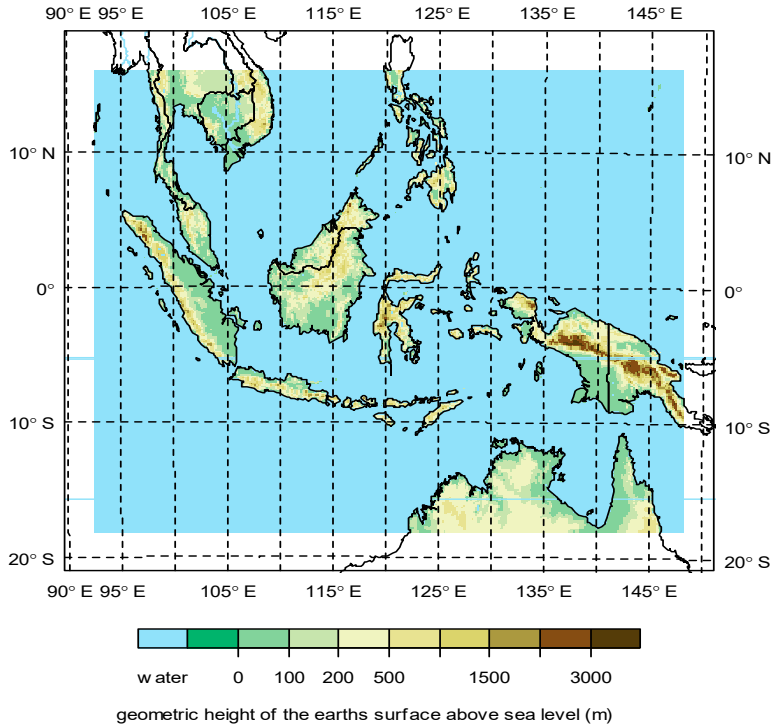

Figure 1. Elevation map of Southeast Asia ranging from 0 m to 3000 m. The area spanning from 14° S to 15° N and 93° E to 138° E is the region for analysis of this study. Blue color corresponds to water points.

2.3. Coupling Concept and Analysis Method

The coupling strength concept was adapted from Sippel et al. [32] and Knist et al. [33] to our study to provide a useful measure of land–atmosphere coupling behavior based on Pearson correlations between the two variables. The coupling concept of this study is exemplified for maximum air temperature, latent heat flux, and soil moisture deficit, as shown in Figure 2, for positive and negative couplings.

1. Positive or "weak" coupling—wet regime where the atmosphere impacts the land: If sufficient soil moisture is available, the maximum air temperature dominates the near-surface atmospheric humidity and latent heat flux and with that the soil moisture. This results in positive correlations between the air temperature and latent heat flux, as well as between latent heat flux and the soil moisture deficit. Here, the atmosphere influences the land, as the soil moisture deficit is not high enough to dominate via soil moisture latent heat flux feedback.
2. Negative or "strong" coupling—dry or transitional regime where land impacts the atmosphere: If sufficient soil moisture is not available, latent heat flux and also near-surface atmospheric humidity is limited by this moisture deficit, resulting in a negative correlation. If latent heat flux decreases, the maximum air temperature increases due to the lower amount of evaporative cooling, resulting in a negative correlation between the two variables. In addition, air temperature

and sensible heat flux increase due to the response to increasing radiation. In this case, the land affects the atmosphere via a decrease in latent heat flux and increases in air temperature and sensible heat flux.

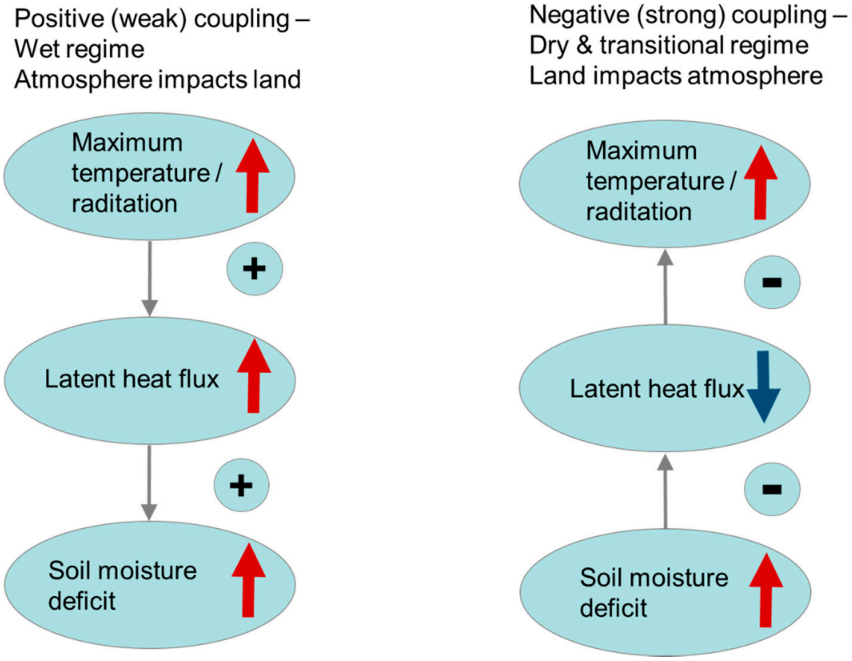

Figure 2. Conceptual coupling diagram between maximum air temperature, latent heat flux, and soil moisture deficit. Correlations are positive for weak positive coupling (left side), and negative for strong negative coupling (right side). Red arrows represent an increase in the respective variables, and blue arrows represent a decrease. Grey arrows represent the direction of coupling.

We considered correlations between the maximum air temperature and latent heat flux to address the soil–moisture–temperature feedback [30] and the feedback into the atmosphere [33]. In cases where land is covered by vegetation, this metric accounts for the moisture flux capability of the vegetation layer. For example, the water transpiration capability of grass is smaller than that of tropical forest. Correlations were calculated between the sensible and latent heat fluxes, as they show the process of the flux partitioning change due to the available energy at the surface. In order to account for the impact of deforestation on the atmospheric boundary layer, we considered the correlations between latent heat flux and the height of the planetary boundary layer.

The coupling correlations were calculated for both the Control and Grass simulations from 10-day mean values of maximum air temperature, latent and sensible heat flux, and planetary boundary layer height from November to March for the full period (1990 to 2004). We chose the period from November to March since this season is less correlated with sea surface temperature patterns [38] and thus is advantageous for a deforestation impact study. In addition, changes in the correlations due to deforestation based on the differences between the Grass and Control simulations (Grass minus Control) were calculated. Correlations were calculated for the strongest El Niño events that occurred during 1991/92, 1994/95, 1997/98, and 2002/03, and for the strongest La Niña events that occurred during 1995/96, 1998/99, 1999/00, and 2000/01. Furthermore, the change in the land–atmosphere coupling due to ENSO events was calculated for the Grass and Control simulations. This was done by calculating the difference in correlations between maximum temperature and the latent heat flux between El Niño and non-El Niño years, and between La Niña and non-La Niña years.

The difference in the surface evaporative fraction of the Grass and Control simulations was calculated in order to attribute the changes in maximum temperature due to deforestation to the changes in the turbulent fluxes. A non-parametric regression method (LOESS) was applied to the changes in surface evaporative fraction and the changes in maximum temperature due

to deforestation. LOESS combines linear least squares regression with the flexibility of nonlinear regression. Simple models are fitted to localized subsets of the data to build up a function that describes the deterministic part of the variation in the data.

The analysis of this study was conducted over land grid points only.

3. Results

3.1. Land–Atmosphere Coupling

The spatial distribution of Pearson correlation coefficients over Southeast Asia is shown in Figure 3 for the period from 1990 to 2004 for November to March. The correlations were calculated based on 10-day means. They describe the latent heat flux and maximum temperature feedback (Figure 3a), the latent and sensible heat flux correlation (Figure 3b), and the latent heat flux and planetary boundary layer height correlation (Figure 3c) for the Control (upper row) and deforestation (Grass) simulations (lower row). The coupling strength between land and atmosphere increased (negative correlations) for all correlations due to deforestation. The coupling strength over the mainland was found to be strongest (Pearson correlation coefficient up to −0.8 and −1). The impact was less pronounced over the maritime islands (Pearson correlation coefficients between −0.2 and −0.8), where the signal due to deforestation is mixed with the influence of the ocean.

The correlations over Sumatra, West of Borneo, and the Northern part of New Guinea were positive in the Control simulation (Figure 3 upper row). These are mainly forested regions in the Control simulation, for which positive correlations were obtained (Pearson correlation coefficient ~0.8). The reason for this is that the latent and sensible heat fluxes are both of high value over forested areas [28], which resulted in positive correlations between these turbulent fluxes. Therefore, correlations between the latent heat flux and maximum temperature were also positive. Due to the lower albedo of forests, more radiation is absorbed and transformed via evapotranspiration to latent heat fluxes and via heat conduction to sensible heat fluxes. The increased radiation and sensible heat fluxes increase the temperature over forested areas, and with that, the maximum temperature increases. Increased heat fluxes over forested areas influence the planetary boundary layer, which was also found to increase [39], leading to positive correlations.

The correlations over Sumatra, West of Borneo, and the Northern part of New Guinea switched from positive to negative correlations over most of these areas for the Grass simulation as compared to the Control simulation (Figure 3 lower row). The latent heat flux decreased after land clearing, reducing the evaporative cooling potential and thereby increasing the maximum temperatures (Figure 3a lower row, and Figure 4b). Further, the increase in sensible heat flux due to deforestation (Figure 3b lower row) induced higher temperatures and heat extremes (also see Figure 4b). The increase in maximum temperature in the Grass simulation [19] was accompanied by a decrease in the latent heat flux due to deforestation, leading to negative correlations. The deepening of the boundary layer increases as less water is added to the atmosphere by evaporation and transpiration, as shown by the negative correlation between latent heat flux and the planetary boundary layer height.

Maximum temperature was warmer after deforestation by 0.4 to 1.8 °C (Figure 4a). The increase in maximum temperature after land clearing is accompanied by decreases in the surface evaporative fraction (Figure 4b). The magnitude of change in extreme temperature due to deforestation depends on the former coupling strength over the region (Figures 3 and 4). The rise in extreme temperatures due to deforestation has occurred mainly over the mainland, where the coupling strength was the strongest (Figure 3a,b). The impact has been less pronounced over the maritime islands due to the oceanic influence, suggesting that the regional-scale impact of deforestation depends on the coupling strength before land clearing. Please note that the analysis is during austral summers where the Asian-Australian Monsoon develops in the southern region of the domain. This is the reason why maximum temperature differences are less pronounced in the south.

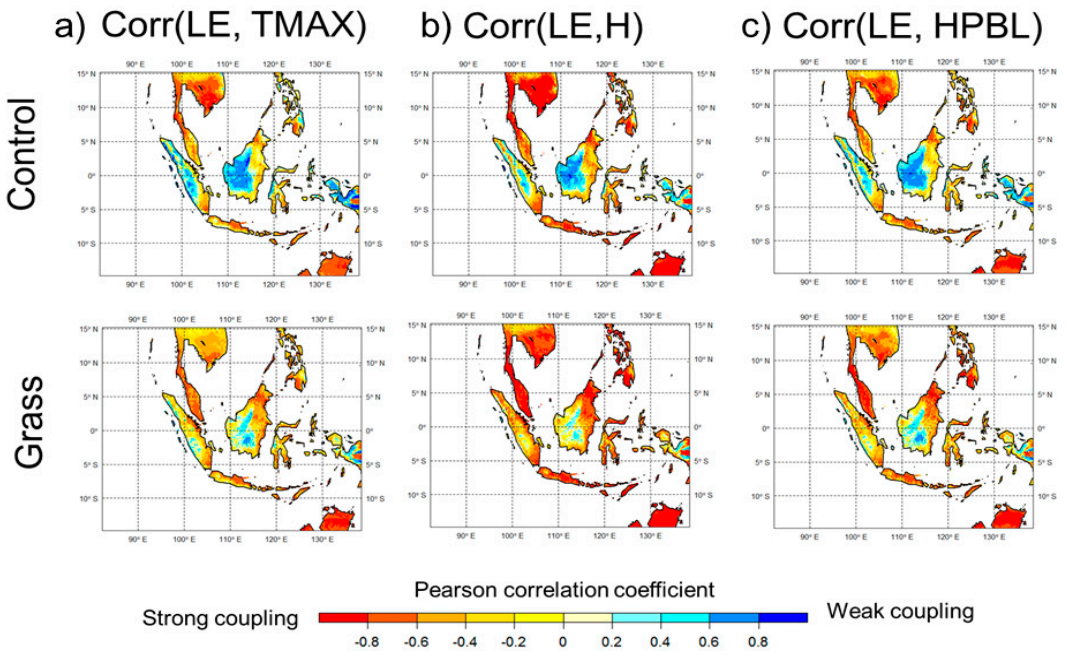

Figure 3. Spatial distribution of Pearson correlation coefficients describing (**a**) the latent heat flux (LE) and maximum temperature (TMAX) feedback, (**b**) the latent (LE) and sensible heat flux (H) correlation, and (**c**) the latent heat flux (LE) and planetary boundary layer height (HPBL) correlation of the Control simulation (upper row) and Grass simulation (lower row) for the period from 1990 to 2004 for November to March. The correlation was calculated based on 10-day means. The analysis was done on land points only.

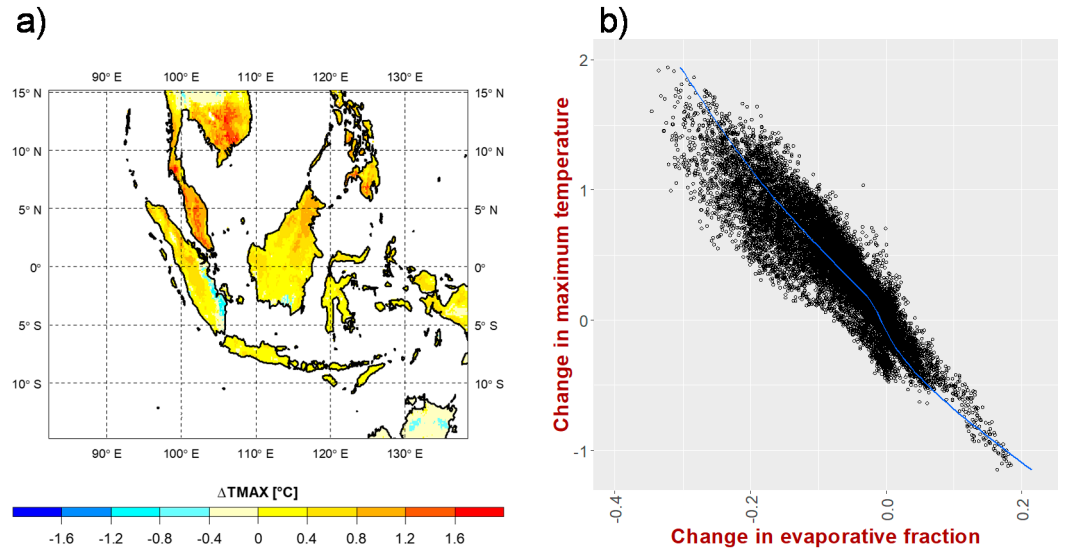

Figure 4. (**a**) Spatial distribution of the maximum temperature (TMAX) differences in degree Celsius between the Control and Grass simulation over Southeast Asia for the years 1990 to 2004 from November to March based on 10-day mean values. (**b**) Scatterplot of the change in surface evaporative fraction versus the change in maximum temperature. The non-parametric regression line is in blue with 95% confidence region in grey. The analysis was conducted on land points only.

3.2. *Coupling Change during El Niño*

The spatial distribution of Pearson correlation coefficients between the latent heat flux and maximum temperature are shown for non-El Niño years (Figure 5a) and the strongest El Niño years (Figure 5b) over Southeast Asia for the years from 1990 to 2004. The correlations were calculated based

on 10-day mean values of the latent heat flux and maximum temperature from November to March. The strongest El Niño events occurred in 1991/92, 1994/95, 1997/98, and 2002/03. The upper row of Figure 5 shows the Control simulation, which was compared with the Grass simulation (lower row in Figure 5). The box plot with a kernel density plot rotated and surrounding it on each side was used to quantify the change in correlation between El Niño and non-El Niño years for the Control simulation (grey) and the Grass simulation (dark red, Figure 5c).

The correlation between maximum temperature and the latent heat flux had stronger coupling for the Grass simulation as compared to the Control simulation (Figure 4a). While maximum temperature increased, the latent heat flux decreased due to deforestation, resulting in more correlations that are negative. The correlation strength intensified and shifted towards stronger coupling during El Niño events for both Control and Grass simulations.

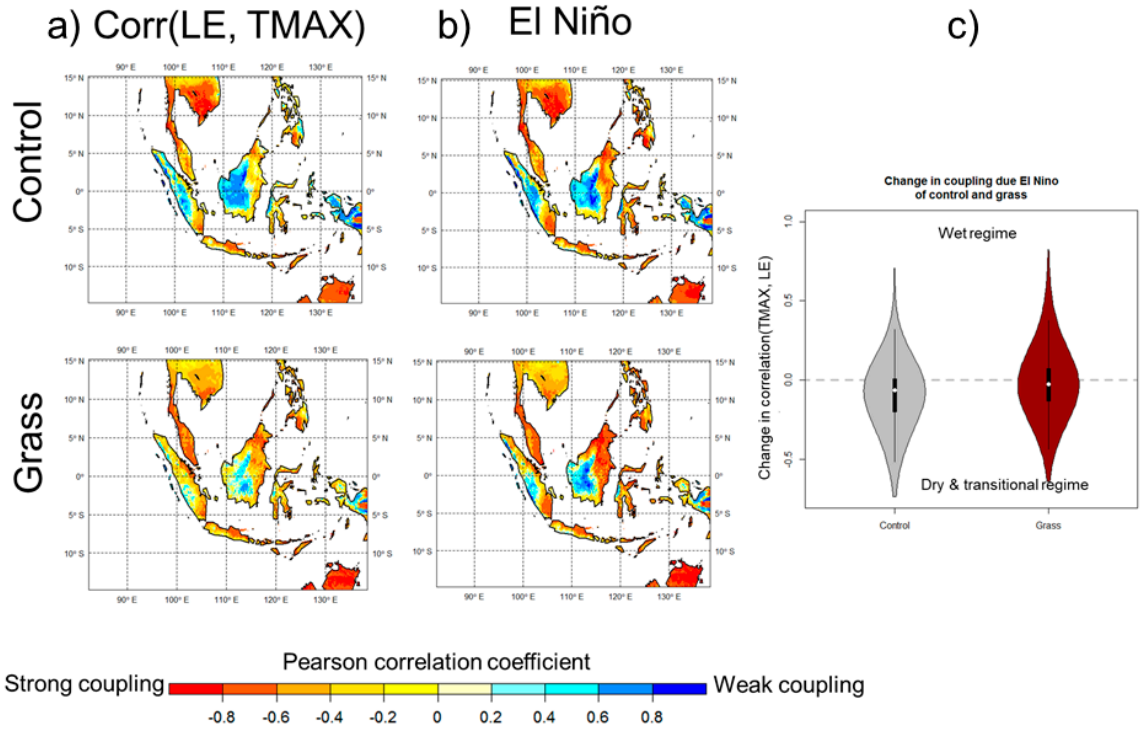

Figure 5. Spatial distribution of the Pearson correlation coefficient for November to March 10-day means of the latent heat flux (LE) and maximum temperature (TMAX) over Southeast Asia for the years 1990 to 2004 from November to March. (**a**) The first column presents the correlation of the variables for the Control and Grass simulations. (**b**) The second column shows the correlations for the Control and Grass simulations during El Niño events. (**c**) The box plot with a kernel density plot rotated and surrounding it on each side quantifies the change in correlation of LE and TMAX between El Niño and non-El Niño years for the Control simulation (grey) and the Grass simulation (dark red). The strongest El Niño events occurred in 1991/92, 1994/95, 1997/98, and 2002/03. The analysis was conducted on land points only.

The box plot shows that the change in correlation due to El Niño phases towards strong coupling was more pronounced for the Control simulation than for the Grass simulation (Figure 5c). This demonstrates that the magnitude in correlation change between maximum temperature and the latent heat flux due to El Niños was higher for the Control simulation as compared to the Grass simulation. The effect of an El Niño phase with drier and warmer conditions than usual did not change the environmental conditions in the Grass simulation as much as in the Control simulation. The reason is that the climate conditions for the Grass simulation were already drier and warmer than for the Control simulation.

3.3. Coupling Change during La Niña

Figure 6 shows the spatial distribution of Pearson correlation coefficients of 10-day means of the latent heat flux and maximum temperature for the years 1990 to 2004 from November to March during non-La Niña (Figure 6a) and the strongest La Niña years (Figure 6b). The upper row of Figure 6 shows the Control simulation, which was compared to the Grass simulation (lower row in Figure 6). The box plot with a kernel density plot rotated and surrounding it on each side was used to quantify the change in correlation between La Niña and non-La Niña years for the Control simulation (grey) and the Grass simulation (dark red, Figure 6c). The strongest La Niña events occurred in the years 1995/96, 1998/99, 1999/00, and 2000/01.

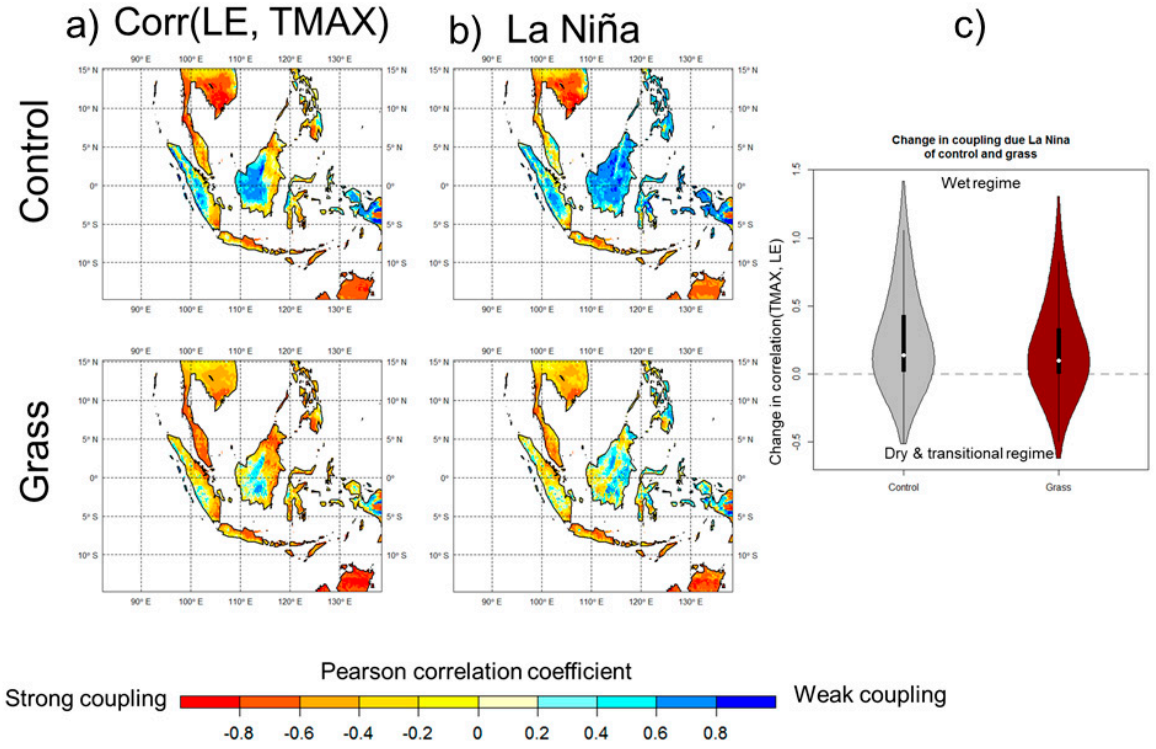

Figure 6. Spatial distribution of the Pearson correlation coefficient of 10-day means of latent heat flux (LE) and maximum temperature (TMAX) over Southeast Asia for the years 1990 to 2004 from November to March. The first column presents the correlation of the variables for the Control and Grass simulation. The second column shows the correlations for the Control and Grass simulations during La Niña events. The box plot with a kernel density plot rotated and surrounding it on each side quantifies the change in correlation of LE and TMAX between La Niña and non La Niña years for the control simulation (grey) and the grass simulation (dark red). The strongest La Niña events occurred in 1995/96, 1998/99, 1999/00, and 2000/01. The analysis was conducted on land points only. (**a**) The first column presents the correlation of the variables for the Control and Grass simulation. (**b**) The second column shows the correlations for the Control and Grass simulations during La Niña events. (**c**) The box plot with a kernel density plot rotated and surrounding it on each side quantifies the change in correlation of LE and TMAX between La Niña and non La Niña years for the control simulation (grey) and the grass simulation (dark red).

The correlation strength reduced and shifted towards weak coupling (positive correlations) during La Niña events for both the Grass and Control simulations (Figure 6a,b). The change in the correlation between La Niña and non-La Niña years towards weak coupling was more pronounced for the Control simulation than for the Grass simulation (Figure 6b,c).

3.4. Coupling Change Due to Deforestation

The changes in coupling between the maximum temperature and latent heat flux due to deforestation during the full time period from 1990 to 2004, during El Niño and La Niña events for November to March, are presented in Figure 7 as a box plot with a kernel density plot rotated and surrounding it on each side. Deforestation changed the correlation towards stronger coupling as shown for the full time period. During La Niña events, changes were the most dramatic, leading to a dry regime, as indicated by the change towards negative correlations and by the change in the mean correlation by 40%. The coupling change due to deforestation during La Niña events was the strongest. The land–atmosphere coupling became stronger due to deforestation. The colder and wetter conditions during La Niña events were shown to be less effective for turning the coupling into a wet regime. The coupling in the Control simulation was weaker over most of the maritime islands, and became even weaker during La Niña events as compared with the Grass simulation. The coupling change during El Niño events was weaker among the three cases (Full period, El Niño, La Niña). Environmental conditions are already drier after land clearing. That is the reason why the effect of El Niño that is associated with warmer temperatures and less rain has only a marginal additional effect on the coupling strength. It is suggested that the impact of deforestation is much stronger than the impact of climate variability in this region. The state of the land surface and land–atmosphere feedback modulate and amplify climate variability.

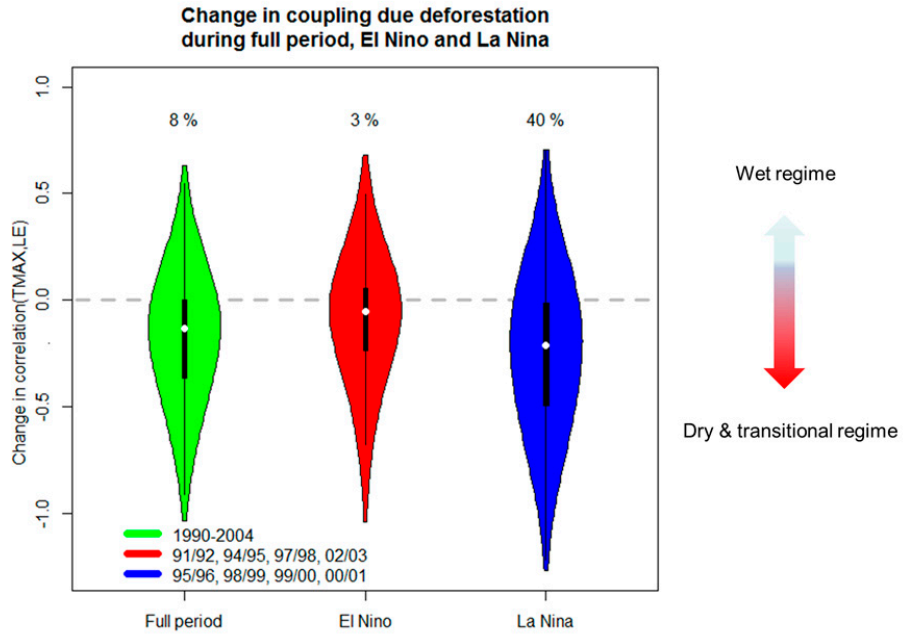

Figure 7. Change in the Pearson correlation coefficient between the maximum temperature (TMAX) and latent heat flux (LE) due to deforestation quantified as a box plot during the full period (green), during the strongest El Niño years (red), and during the strongest La Niña years (blue) from 1990 to 2004 for November to March over Southeast Asia. Shown is a box plot with a kernel density plot rotated and surrounding it on each side. The mean change rate of the Pearson correlation coefficient as a percentage is displayed above each box plot. The analysis was conducted on land points only.

4. Summary and Conclusions

Southeast Asia's deforestation is occurring at a fast pace due to an increase in use of land for agriculture and urban development. The impact of deforestation on the land–atmosphere coupling strength was assessed in this study by analyzing ERA-Interim-driven simulations of the state-of-the-art regional climate model COSMO-CLM during the period from 1990 to 2004 for November to March. The impact of land clearing during ENSO events was examined as well.

The coupling strength concept helps to determine whether the land surface conditions affect the atmosphere via evapotranspiration processes (strong coupling/negative correlations) or whether the atmosphere affects the land surface by temperature and radiation (weak coupling/positive correlations). This is useful information that also relates to climate change. Furthermore, this concept could be used in land cover change studies to determine the impact of deforestation on the climate and climate variability.

Pearson correlations between two variables were calculated to represent the coupling strength from 1990 to 2004, during El Niño and La Niña events. Pearson correlations and correlation changes due to deforestation and ENSO were calculated between the latent heat flux and maximum temperature, the latent and sensible heat flux, and the latent heat flux and the planetary boundary layer height. The coupling strength between land and atmosphere was shown to increase, leading to stronger coupling (negative correlations) among all correlations due to deforestation. This implies a strong impact of the land on the atmosphere after deforestation.

Differences in environmental conditions due to deforestation are most effective during La Niña years. Generally, environmental conditions in SEA during La Niña events are wetter and colder than usual. Deforestation has a strong effect by changing the environmental conditions in this time period to drier and warmer conditions than usual [19]. Maximum temperatures increase due to deforestation, which depends on the coupling strength of the maximum temperature and the latent heat flux over the region. The change in coupling (correlation) is a movement toward negative coupling (strong) due to deforestation. The wet and cold conditions due the atmospheric circulation during La Niña phases are superimposed by the impact of the land on the atmosphere. This reduces the strength of La Niña events on the region.

The correlation strength intensified and shifted towards stronger coupling during El Niño events for both Control and Grass simulations. The change in correlation due to El Niño phases towards strong coupling was more pronounced for the Control simulation than for the Grass simulation. El Niño years have the potential to become warmer and drier than during usual conditions without deforestation. This study showed that deforestation amplifies the strength of El Niño events on the region.

The changed conditions due to deforestation could favor an increase in the formation of tropical cyclones. The physical mechanism that leads to an increase in tropical cyclones is mainly vertical wind shear. Wind shear only weakly develops during El Niño events in the tropical Pacific [23], which favors the formation of tropical cyclones. Such an outcome of deforestation could lead to significant socioeconomic consequences [26] and unprecedented environmental impacts affecting health, productivity, crop yield, and disease outbreaks for the growing population in the coastal areas of SEA [27].

Whether deforestation will lead to a permanent transition to agricultural production in this region cannot be concluded. Rather, deforestation in the Southeast Asian region increases the vulnerability to droughts and heat extremes. This can potentially lead to additional forest loss and decreases in agricultural productivity. The use of large-scale deforestation as the maximum possible deforestation scenario in this study changed the land–atmosphere coupling from an atmosphere-dominated coupling to a land-dominated one. Deforestation modifies the land surface properties, resulting in alterations to surface fluxes such as moisture, heat, and momentum, affecting the atmospheric boundary layer [40]. The consequences of deforestation are a drier climate regime in the Southeast Asian region through positive feedback processes, which amplifies climate variability [41,42]. The magnitude of change in environmental conditions due to deforestation depends on the coupling strength before land clearing.

Last but not least, deforestation for agricultural production in the Southeast Asian region significantly increases CO_2 emissions, directly contributing to global warming, of which soil microbial processes have the greatest contribution [42]. Rising temperatures due to deforestation have the potential to decrease net primary production, given the need to increase fertilizer application to stabilize crop production. This approach additionally releases nutrients to the ocean, increasing eutrophication or nitrous oxides released into the atmosphere, the latter acting as greenhouse gases. Besides nutrients, crops also need water, but water stress onset might become more frequent with deforestation.

Although the analysis is based on an idealized case study of a regional climate model with rather coarse horizontal resolution of 14 km, it shows the potential trends in environmental conditions if current deforestation rates continue.

Thus, the impact of deforestation will be another threat in addition to global warming in the next decades due to the increase in the occurrence of multiple extreme events [43]. This may change the type and severity of upcoming impacts on the vulnerability and sustainability of our society. Further regional climate modelling studies, including land management, are needed to strengthen the results and to quantify the impact for the longer term in the future.

Author Contributions: Conceptualization, M.H.T.; data curation, M.H.T.; formal analysis, M.H.T.; investigation, M.H.T.; methodology, M.H.T.; resources, M.H.T.; software, M.H.T.; validation, M.H.T.; visualization, M.H.T.; writing—original draft, M.H.T.; writing—review and editing, M.H.T. The author has read and agreed to the published version of the manuscript.

Funding: This research recieved no external funding.

Acknowledgments: This research was part of research related to the project CRC990 Ecological and Socioeconomic Functions of Tropical Lowland Rainforest Transformation Systems (EFForTS) under the support of the German Research Foundation (DFG). Computational resources were made available by the German Climate Computing Center (DKRZ) through support from the German Federal Ministry of Education and Research (BMBF). We acknowledge the funding of the German Research Foundation (DFG) through grant nr. 401857120.

Conflicts of Interest: The author declares no conflict of interest.

References

1. IPCC. Contribution of Working Groups I, II and III to the Fifth Assessment Report of the Intergovernmental Panel on Climate Change. In *Climate Change 2014: Synthesis Report*; Pachauri, R.K., Meyer, L.A., Eds.; IPCC: Geneva, Switzerland, 2014; 151p. Available online: https://www.ipcc.ch/pdf/assessment-report/ar5/syr/SYR_AR5_FINAL_full_wcover.pdf (accessed on 1 May 2020).
2. Stocker, T.F.; Qin, D.; Plattner, G.-K.; Alexander, L.V.; Allen, S.K.; Bindoff, N.L.; Bréon, F.-M.; Church, J.A.; Cubasch, U.; Emoir, S.; et al. Contribution of Working Group I to the Fifth Assessment Report of the Intergovernmental Panel on Climate Change. In *Climate Change 2013: The Physical Science Basis*; Technical Summary; Stocker, T.F., Qin, D., Plattner, G.-K., Tignor, M., Allen, S.K., Boschung, J., Nauels, A., Xia, Y., Bex, V., Midgley, P.M., Eds.; Cambridge University Press: Cambridge, UK, 2013. Available online: https://www.ipcc.ch/site/assets/uploads/2018/02/WG1AR5_TS_FINAL.pdf (accessed on 1 May 2020).
3. Chape, S.; Spalding, M.; Jenkins, M.D. *The World's Protected Areas*; UNEP World Conservation Monitoring Centre; University of California Press: Berkeley, CA, USA, 2008.
4. Huang, C.; Goward, S.N.; Schleeweis, K.; Thomas, N.; Masek, J.; Zhu, Z. Dynamics of national forests assessed using the Landsat record: Case studies in eastern United States. *Remote Sens. Environ.* **2009**, *113*, 1430–1442. [CrossRef]
5. Hansen, M.C.; Potapov, P.V.; Moore, R.; Hancher, M.; Turubanova, S.A.; Tyukavina, A.; Thau, D.; Stehman, S.V.; Goetz, S.J.; Loveland, T.R.; et al. High-resolution global maps of 21st-century forest cover change. *Science* **2013**, *342*, 850–853. [CrossRef]
6. Margono, B.A.; Potapov, P.V.; Turubanova, S.; Stolle, F.; Hansen, M.C. Primary forest cover loss in Indonesia over 2000–2012. *Nat. Clim. Chang.* **2014**, *4*, 730–735. [CrossRef]
7. McGrath, M.J.; Luyssaert, S.; Meyfroidt, P.; Kaplan, J.O.; Bürgi, M.; Chen, Y.; Erb, K.; Gimmi, U.; McInerney, D.; Naudts, K.; et al. Reconstructing European forest management from 1600 to 2010. *Biogeosciences* **2015**, *12*, 4291–4316. [CrossRef]
8. Estoque, R.C.; Ooba, M.; Avitabile, V.; Hijioka, Y.; DasGupta, R.; Togawa, T.; Murayama, Y. The future of Southeast Asia's forests. *Nat. Commun.* **2019**. [CrossRef]
9. Gaveau, D.L.A.; Locatelli, B.; Salim, M.A.; Yaen, H.; Pacheco, P.; Sheil, D. Rise and fall of forest loss and industrial plantations in Borneo (2000–2017). *Conserv. Lett.* **2018**. [CrossRef]
10. Oettli, P.; Behera, S.K.; Yamagata, T. Climate Based Predictability of Oil Palm Tree Yield in Malaysia. *Sci. Rep.* **2018**, 8. [CrossRef]
11. Bonan, G.B. Forests and Climate Change: Forcings, Feedbacks, and the Climate Benefits of Forests. *Science* **2008**, *320*, 1444–1449. [CrossRef]

12. Pielke, R.A.; Pitman, A.J.; Niyogi, D.; Mahmood, R.; McAlpine, C.; Hossain, F.; Goldewijk, K.K.; Nair, U.S.; Betts, R.; Fall, S.; et al. Land use/land cover changes and climate: Modeling analysis and observational evidence. *Clim. Chang.* **2011**, *2*, 828–850. [CrossRef]
13. Pielke, R.A.; Avissar, R.; Raupach, M.; Dolman, A.J.; Zeng, X.B.; Denning, A.S. Interactions between the atmosphere and terrestrial ecosystems: Influence on weather and climate. *Glob. Chang. Biol.* **1998**, *4*, 461–475. [CrossRef]
14. Mahmood, R.; Pielke, R.A., Sr.; Hubbard, K.G.; Niyogi, D.; Dirmeyer, P.A.; McAlpine, C.; Carleton, A.M.; Hale, R.; Gameda, S.; Beltrán-Przekurat, A.; et al. Land cover changes and their biogeophysical effects on climate. *Int. J. Clim.* **2014**, *34*, 929–953. [CrossRef]
15. Liu, S.; Bond-Lamberty, B.; Boysen, L.R.; Ford, J.D.; Fox, A.; Gallo, K.; Hatfield, J.; Henebry, G.M.; Huntington, T.; Liu, Z.; et al. Grand challenges in understanding the interplay of climate and land changes. *Earth Interact.* **2017**, *21*, 1–43. [CrossRef]
16. Heald, C.L.; Spracklen, D.V. Land use change impacts on air quality and climate. *Chem. Rev.* **2015**, *115*, 4476–4496. [CrossRef]
17. Spracklen, D.V.; Baker, J.C.A.; Garcia-Carreras, L.; Marsham, J. The Effects of Tropical Vegetation on Rainfall. *Annu. Rev. Environ. Resour.* **2018**, *43*, 193–218. [CrossRef]
18. Tölle, M.H.; Gutjahr, O.; Thiele, J.; Busch, G. Increasing bioenergy production on arable land: Does the regional and local climate respond? Germany as a case study. *J. Geophys. Res. Atmos.* **2014**, *119*, 2711–2724. [CrossRef]
19. Tölle, M.H.; Engler, S.; Panitz, H.-J. Impact of abrupt land cover changes by tropical deforestation on South-East Asian climate and agriculture. *J. Clim.* **2017**, *30*, 2587–2600. [CrossRef]
20. Kovats, R.S.; Bouma, M.J.; Hajat, S.; Worrall, E.; Haines, A. El Niño and health. *Lancet* **2003**, *362*, 1481–1489. [CrossRef]
21. Zhao, H.; Wang, C. Interdecadal modulation on the relationship between ENSO and typhoon activity during the late season in the western North Pacific. *Clim. Dyn.* **2016**, *47*, 315–328. [CrossRef]
22. Zhan, R.; Wang, Y.; Zhao, J. Intensified Mega-ENSO Has Increased the Proportion of Intense Tropical Cyclones over the Western Northwest Pacific since the Late 1970s. *Geophys. Res. Lett.* **2017**, *44*, 11959–11966. [CrossRef]
23. Mei, W.; Xie, S.-P.; Primeau, F.; MCWilliams, J.C.; Pasquero, C. Northwestern Pacific typhoon intensity controlled by changes in ocean temperatures. *Sci. Adv.* **2015**, *1*, e1500014. [CrossRef]
24. Mei, W.; Xie, S.-P. Intensification of land falling typhoons over the northwest Pacific since the late 1970s. *Nat. Geosci.* **2016**, *9*, 753–759. [CrossRef]
25. Meehl, G.A.; Stocker, T.F.; Collins, W.D.; Friedlingstein, P.; Gaye, A.T.; Gregory, J.M.; Kitoh, A.; Knutti, R.; Murphy, J.M.; Noda, A.; et al. Contribution of Working Group I to the Fourth Assessment Report of the Intergovernmental Panel on Climate Change. In *Climate Change 2007: The Physical Science Basis*; Global Climate Projections; Solomon, S., Qin, D., Manning, M., Chen, Z., Marquis, M., Averyt, K.B., Tignor, M., Miller, H.L., Eds.; Cambridge University Press: Cambridge, UK, 2007.
26. Welker, C.; Faust, E. Tropical cyclone-related socio-economic losses in the western North Pacific region. *Nat. Hazards Earth Syst. Sci.* **2013**, *13*, 115–124. [CrossRef]
27. Mei, W.; Xie, S.-P.; Primeau, F.; McWilliams, J.C.; Pasquero, C. Global warming hiatus contributed to the increased occurrence of intense tropical cyclones in the coastal regions along East Asia. *Sci. Rep.* **2018**, *8*, 6023. [CrossRef]
28. Tölle, M.H.; Breil, M.; Radtke, K.; Panitz, H.-J. Sensitivity of European temperature to albedo parameterization in the regional climate model COSMO-CLM linked to extreme land use change. *Front. Environ. Sci.* **2018**. [CrossRef]
29. McAlpine, C.A.; Johnson, A.; Salazar, A.; Syktus, J.; Wilson, K.; Meijaard, E.; Seabrook, L.; Dargusch, P.; Nordin, H.; Sheil, D. Forest loss and Borneo's climate. *Environ. Res. Lett.* **2018**, *13*, 044009. [CrossRef]
30. Seneviratne, S.I.; Corti, T.; Davin, E.L.; Hirschi, M.; Jaeger, E.B.; Lehner, I.; Orlowsky, B.; Teuling, A.J. Investigating soil moisture–climate interactions in a changing climate: A review. *Earth Sci. Rev.* **2010**, *99*, 125–161. [CrossRef]
31. Goddard, L. From science to service. *Science* **2016**, *353*, 1366–1367. [CrossRef] [PubMed]

32. Sippel, S.; Zscheischler, J.; Mahecha, M.D.; Orth, R.; Reichstein, M.; Vogel, M.; Seneviratne, S.I. Refining multi-model projections of temperature extremes by evaluation against land-atmosphere coupling diagnostics. *Earth Syst. Dyn.* **2017**, *8*, 387–403. [CrossRef]
33. Knist, S.; Goergen, K.; Buonomo, E.; Christensen, O.B.; Colette, A.; Cardoso, R.M.; Fealy, R.; Fernandez, J.; Garcia-Diez, M.; Jacob, D.; et al. Land-atmosphere coupling in EURO-CORDEX evaluation experiments. *J. Geophys. Res. Atmos.* **2017**, *122*, 79–103. [CrossRef]
34. Margono, B.A.; Turubanova, S.; Zhuravleva, I.; Potapov, P.; Tyukavina, A.; Baccini, A.; Goetz, S.; Hansen, M.C. Mapping and monitoring deforestation and forestdegradation in Sumatra (Indonesia) using Landsat timeseries data sets from 1990 to 2010. *Environ. Res. Lett.* **2012**, *7*, 034010. [CrossRef]
35. Doms, G.; Förstner, J.; Heise, E.; Herzog, H.-J.; Raschendorfer, M.; Schrodin, R.; Reinhardt, T.; Vogel, G. *A Desciption of the Nonhydrostatic Regional Model LM. Part II: Physical Parametrization*; Technical Report; Deutscher Wetterdienst: Offenbach, Germany, 2005; 133p.
36. Rockel, B.; Will, A.; Hense, A. The regional climate model COSMO-CLM (CCLM). *Meteorol. Z.* **2008**, *17*, 347–348. [CrossRef]
37. Dee, D.P.; Uppala, S.M.; Simmons, A.J.; Berrisford, P.; Poli, P.; Kobayashi, S.; Andrae, U.; Balmaseda, M.A.; Balsamo, G.; Bauer, D.P.; et al. The ERA-Interim reanalysis: Configuration and performance of the data assimilation system. *Q. J. R. Meteorol. Soc.* **2011**, *137*, 553–597. [CrossRef]
38. Hendon, H.H. Indonesian rainfall variability: Impacts of ENSO and local air–sea interaction. *J. Clim.* **2003**, *16*, 1775–1790. [CrossRef]
39. Teuling, A.J.; Taylor, C.M.; Meirink, J.F.; Melsen, L.A.; Miralles, D.G.; van Heerwarden, C.C.; Vautard, R.; Stegehuis, A.I.; Nabuurs, G.-J.; Vila-Guerau de Arellano, J. Observational evidence for cloud cover enhancement over western European forests. *Nat. Commun.* **2017**. [CrossRef]
40. Pielke, R.A. Influence of the spatial distribution of vegetation and soils on the prediction of cumulus convective rainfall. *Rev. Geophys.* **2001**, *39*, 151–177. [CrossRef]
41. Dickinson, R.E. How the coupling of the atmosphere to ocean and land helps determine the timescales of interannual variability of climate. *J. Geophys. Res.* **2000**, *105*, 20115–20119. [CrossRef]
42. Vereecken, H.; Schnepf, A.; Hopmans, J.; Javaux, M.; Or, D.; Roose, T.; VanderBorght, J.; Young, M.; Amelung, W.; Aitkenhead, M.; et al. Modeling Soil Processes: Review, Key Challenges, and New Perspectives. *Vadose Zone J.* **2016**, 15. [CrossRef]
43. Wang, G.; Eltahir, E.A. Biosphere-atmosphere interactions over West Africa, II, Multiple climate equilibria. *Q. J. R. Meteorol. Soc.* **2000**, *126*, 1261–1280. [CrossRef]